Optimization of Co-flow Micro-heat-exchanger Performance Using Response Surface Methodology: Energy Transfer Rate and Thermodynamic Irreversibility

Mokhtar Ferhi
Assistant Professor
UR22ES12: Modeling, Optimization and Augmented Engineering, ISLAIB, University of Jendouba, Beja 9000
Tunisia

Bouchmel Mliki
Assistant Professor
CORIA, Normandie Université, INSA de Rouen, Technopôle du Madrillet, BP 8
Saint-Etienne-du-Rouveray 76801
France

Rached Miri
Assistant Professor
Research Laboratory, Technology, Energy and Innovative Materials, Faculty of Science, University of Gafsa
Tunisia

Ridha Djebali
Full Professor
UR22ES12: Modeling, Optimization and Augmented Engineering, ISLAIB, University of Jendouba, Beja 9000
Tunisia

This paper investigates the optimization of energy transfer rates and minimization of thermodynamic irreversibility in a co-flow microchannel heat exchanger using Response Surface Methodology (RSM) coupled with a Box-Behnken Design of Experiments. A surrogate model is developed to correlate critical input parameters—including Reynolds number (Re), Knudsen number (Kn), volume fraction (Vf), and particle diameter (Dp)—with the system responses: average Nusselt number (Nu_avg) and entropy generation (S_gen). The study explicitly addresses the effects of inlet flow conditions on thermal performance by analyzing shear-driven forced convection mechanisms. As highlighted in the boundary conditions, velocity gradients at the inlet create a mixing-dominated environment, where the Reynolds number (Re) governs fluid dynamics and heat transfer. This shear-enhanced mixing significantly improves thermal transport, while temperature gradients at the inlet contribute to localized heat exchange between the channel's bottom and top surfaces. The impacts of input parameters are evaluated through velocity profiles, slip velocity, temperature jump, heat transfer rates, and entropy generation. The interplay between these factors reveals that higher Re (linked to increased inlet velocities) intensifies convective heat transfer but also elevates viscous dissipation, presenting a trade-off between Nu_avg and S_gen. RSM optimization identifies Pareto-optimal conditions that maximize heat transfer while minimizing irreversibility. Analysis of Variance (ANOVA) validates the significance of each parameter, yielding regression equations for Nu_avg and S_gen. The results demonstrate RSM's efficacy in balancing competing objectives, offering actionable insights for designing high-efficiency microchannel heat exchangers in applications demanding precise thermal management with minimal energy losses. This work underscores the critical role of inlet flow conditions in dictating microchannel performance, bridging the gap between idealized models and practical operational constraints.

Keywords: *SRT-BGK, optimization, co-flow, correlation, heat transfer, entropy generation, design factors.*

1. INTRODUCTION

Nowadays, the need for very high energy efficiency has resorted to the use of micro-heat-exchangers due to the heat transfer rate which they provide for a very small exchange surface. Face to this challenge and to improve the thermal performance of these MEMS researchers use the response surface methodology [1–10] to maximize the exchanged heat transfer and reduce the entropy generation production inside a micro-heat-exchanger.

To determine the optimum values several input design monitoring factors are combined. Based on the literature review several numerical and experimental have been performed to achieve maximum heat transfer. In this context, many researchers optimize the different configurations of micro-heat-exchangers by combining different design factors [7,11–18]. In microscale systems, enhancing the energy transfer rate (quantified by Nusselt number, Nu) often conflicts with minimizing thermodynamic irreversibility (measured by entropy generation, S_gen). While higher heat transfer is desirable, it can increase viscous dissipation or thermal gradients, raising S_gen. Thus, optimization requires a trade-off between these competing objectives, as demonstrated in prior studies [18–20].

Micro-scale heat exchanger systems have been the focus of many researchers over the past few decades for their wide utilization in micro-channel heat exchangers, micro heat pipes, electronic cooling problems, compact heat exchanger systems, solar collector systems, etc. This is mainly attributed to the increasing demand for

Received: March 2025, Accepted: June 2025
Correspondence to: Assistant Professor Mokhtar Ferhi
UR22ES12: Modeling, Optimization and Augmented Engineering, University of Jendouba, Beja, Tunisia.
E-mail: moktar.ferhi@gmail.com
doi: 10.5937/fme2503409F

reducing the size and weight of these heat exchangers while providing a high heat transfer performance per unit volume by choosing the optimal working fluids and materials. The operating and geometric parameters influencing the performance of the heat exchanger can be scaled to the required dimensions to achieve the desired heat transfer rates and thermal performance. The investigation of micro-heat-exchanger systems is a key area in the field of research in relation to the dimensional reduction of heat transfer equipment. Such systems have limited applications compared to large-scale systems, and they can be integrated to produce cost-effective and compact devices.

In many engineering applications, the performance of energy transfer systems is of critical importance. The efficiency of such systems is often represented by the thermodynamic irreversibility rate. The performance of the co-flow for micro-channel heat exchangers. The co-flow arrangement can maintain steady, non-oscillating heat transfer performance at low flow rates. There exists a range of various parameters such as Reynolds number, Knudsen number, Volume fraction, and Diameter of nanoparticles, for which the heat transfer is maximum and the entropy generation is minimum for the co-flow arrangement.

The thermally developing heat transfer on the co-flow design occurs at a slower rate. The long entrance length in the co-flow heat exchanger minimizes the design and manufacturing complexities by reducing the length and global thermal resistance of the heat exchanger. Preliminary information about the co-flow design finds its application in information and cooling technologies, electronic cooling, solar thermal systems, etc. Miniaturization affects not only the properties of micro-heat-exchangers but also the energy transfer rates. Because of these reasons, many results obtained using various theoretical tools do not have further extrapolative significance and/or the adaptive optimizations with respect to different constraints and are often computed within simplified settings which are, however, by no means representative of real or practical cases that have some thermal peculiarities related to bed heat treatment. In particular, regarding the fully time-dependent transfer relations and timelines of the process inputs, mass-transport coupled heat exchangers become subject to additional control. Therefore, in the present context, the co-flow of two reactive flows flowing under an isothermal temperature drop can involve multi-objective trade-off analysis which are connected as a function of maximum and essentially different characteristics of flow performance, influencing both the energy of the system and the irreversibility.

Recently, to solve the governing equation inside a micro-heat-exchanger, many researchers have used the Lattice Boltzmann method as a new alternative [17,21–23]. Due to the simplicity of coding and his second order in time and space, the lattice Boltzmann method replaces several traditional CFD methods [24,25]. The D_2Q_9 LB model is used in the continuous and slip regimes.

While recent advances in nanofluid microchannel optimization are notable, critical gaps remain. First, RSM applications often target macro-scale systems ([7,11]), overlooking slip-flow regimes ($Kn > 0.001$) prevalent in micro-devices. Second, nanoparticle effects are frequently idealized ([13]), neglecting aggregation-induced losses. Third, single-objective approaches ([10]) fail to address the inherent trade-off between Nu and Sgen. This study bridges these gaps by integrating LBM (for rarefaction-accurate modeling) with RSM to optimize co-flow micro-heat-exchangers, explicitly balancing heat transfer enhancement and irreversibility minimization.

Study	Shortcoming	Our improvement
Javadpour et al.[11]	Macro-scale fins ignore Kn effects	LBM for slip-flow microchannels
Fadodun et al. [13]	Assumes perfect nanofluid dispersion	Empirical nanofluid properties
Pattnaik et al. [26]	Optimizes only Nu	Multi-objective Nu + Sgen RSM
Rabhi et al. [27]	Single-phase flow analysis	Co-flow nanofluid with thermal stability

1.1 Motivation

The drive to enhance thermal management in compact systems necessitates optimizing micro-heat-exchangers (MHEXs), where co-flow configurations offer inherent design advantages. However, maximizing the energy transfer rate (quantified by Nusselt number, *Nu_avg*) in these microscale devices often conflicts with min–imizing thermodynamic irreversibility (quantified by entropy generation, *S_gen*), as viscous dissipation and thermal losses become significant. Prior studies ([2,11,19]) highlight this fundamental trade-off: stra–tegies boosting *Nu_avg* (e.g., higher nanoparticle loa–ding or complex geometries) frequently exacerbate *S_gen*, compromising overall system efficiency and sustainability. Furthermore, optimizing MHEXs is uniquely challenging due to dominant microscale effects like rarefaction (slip flow, $Kn > 0.001$) and conjugate heat transfer, which are inadequately addressed in mac–ro-scale optimizations ([1,7]) or single-objective appro–aches ([2,26]). Therefore, there is a compelling need for a robust methodology capable of navigating this comp–lex multi-objective design space - specifically targeting co-flow MHEXs - to simultaneously maximize heat removal and minimize exergy destruction, thereby un–locking their full potential for high-effi–ciency, compact thermal systems.

1.2 Contributions

This study reframes the optimization challenge for co-flow micro-heat-exchangers by employing Response Surface Methodology (RSM) to perform a rigorous multi-objective trade-off analysis between heat transfer enh–ancement (quantified by Nusselt number, *Nu_avg*) and thermodynamic efficiency (quantified by entropy gene–ration rate, *S_gen*). Rather than pursuing an oversim–plified simultaneous maximization of *Nu_avg* and mini–mization of *S_gen*, the work focuses on identifying Pareto-optimal operating conditions – configurations where *Nu_avg* cannot be significantly increased without incurring a disproportionate rise in *S_gen*, and vice versa. The results critically reveal the nature of the compromise between these competing objectives: under certain parameters (e.g., high Reynolds number, *Re*), maximizing *Nu_avg* necessitates accepting significantly higher *S_gen*, indicating a near-mutually exclusive relationship. Crucially, however, the analysis identifies specific, context-dependent sweet spots where a favorable balance is achievable. For ins–tance, at *Re*=30.7 and *Kn*=0.1, the configuration delivers a substantially improved compromise – offering high heat transfer rates while maintaining *S_gen* at manageable levels – compared to other regimes like *Re*=50. This approach provides designers with actionable insights into parameter combinations that optimally balance performance and efficiency for specific microchannel applications.

1.3 Novelty of this study

This work introduces significant methodological and conceptual novelty by pioneering the integrated application of the Lattice Boltzmann Method (LBM) and Response Surface Methodology (RSM) for the multi-objective optimization of co-flow micro-heat-exchangers (MHEXs) under rarefied gas conditions ($Kn > 0.001$). Specifically, it uniquely addresses the simultaneous maximization of energy transfer rate (quantified by Nusselt number, *Nu*_avg) and minimization of thermodynamic irreversibility (quantified by entropy generation, *S_gen*) within this complex regime. Unlike previous studies that optimized macro/mini-channels ([1,7]), neglected slip-flow effects crucial for true microchannels ([19]), or employed single-objective approaches unable to resolve the inherent *Nu_avg* vs. *S_gen* trade-off ([2,11,26]), this study explicitly models conjugate heat exchange in steady co-flow geometry using LBM to capture rarefaction physics accurately. The core novelty lies in leveraging these high-fidelity LBM simulations to generate the data driving a robust RSM framework, enabling the efficient exploration of the complex design space (spanning Reynolds number, Knudsen number, nanoparticle concentration, etc.) to identify Pareto-optimal solutions that practically balance the competing objectives. This approach successfully identifies novel operating points (e.g., *Re*=30.7, *Kn*=0.1) achieving a critical compromise between high heat transfer and low entropy generation – a key advancement beyond designs solely prioritizing *Nu_avg* ([11]) or neglecting nanofluid-microchannel synergy under slip ([28]).

2. PROBLEM SETTING

Specific engineering application

The analyzed co-flow micro-heat-exchanger is primarily designed for applications requiring compact, high-efficiency thermal management, such as:

- **Microelectronics Cooling**
  - **Application:** Thermal management of CPUs, GPUs, and power electronics in compact devices (e.g., smartphones, IoT sensors).
  - **Relevance:**
    - ✓ The optimized *Re*=30.7, *Kn*=0.1, *Vf*=0.04, and *Dp*=10 nm condition balances heat transfer and energy losses, preventing overheating while minimizing cooling power.
    - ✓ Nanofluid use (Al_2O_3/water): Enhances thermal conductivity by ~20% compared to pure water ([19]).
- **Energy-efficient HVAC systems**
  - **Application:** Microchannel heat exchangers in miniaturized heat pumps or building climate control.
  - **Relevance:**
    - ✓ Co-flow stability reduces temperature oscillations, improving system longevity.
    - ✓ Low *S_gen* (16.8 W/m²K) design cuts energy waste, aligning with sustainable HVAC standards.
- **Biomedical devices**
  - **Application:** Lab-on-a-chip systems for PCR machines or drug delivery.
  - **Relevance:**
    - ✓ Slip-flow regime (*Kn*=0.1) ensures precise temperature control in microfluidic channels.
    - ✓ Nanoparticle diameter (*Dp*=10 nm) avoids clogging in micron-scale channels.
- **Aerospace thermal control**
  - **Application:** Cooling avionics or satellite components in weight-constrained environments.
  - **Relevance:**
    - ✓ Microscale design ($H \approx 100$–500 μm) reduces system mass.
    - ✓ MEMS compatibility (via LBM-validated slip flow) suits low-gravity conditions.
- **Solar thermal collectors**
  - **Application:** Nanofluid-based microchannel absorbers for concentrated solar power.
  - **Relevance:**
    - ✓ High *Nu* (~30.8) maximizes energy capture.
    - ✓ Low *Dp* (10 nm) minimizes nanoparticle sedimentation in stagnant zones.
- **Implementation roadmap**
  - Prototyping: Fabricate microchannels with laser etching or 3D printing.
  - Nanofluid Preparation: Use ultrasonication to stabilize Al_2O_3/water nanofluids at *Vf*=0.04.
  - System Integration: Pair with micro-pumps (e.g., piezoelectric actuators) for Re≈30 flow control.
- **Industry impact**
  - Electronics: Enables thinner laptops/phones with better heat dissipation.
  - Energy: Reduces HVAC operational costs by ~15% via lower *S_gen*.
  - Biotech: Enhances accuracy of portable diagnostic devices.
  -

Principle & purpose:

– The exchanger uses nanofluid flow (nanoparticles in base fluid) to enhance heat transfer via improved thermal conductivity.

– Co-flow configuration (parallel streams of hot/cold fluids) minimizes thermal oscillations, ensuring steady heat exchange.
– Optimization goal: Maximize *Nu_avg* (heat trans–fer) while minimizing *S_gen* (entropy generation, i.e., energy losses).

Geometric definition

The studied micro-heat-exchanger consists of a 2D microchannel driven by a co-flow filled with nano liquid (Figure 1):

- **Height (H)**: Characteristic microscale dimension (e.g., 100–500 µm).
- **Length (L)**: Typically >> H for fully developed flow, taken here L=4H with outflow boundary conditions to prevent recirculations at outlet: The outflow boundary condition is obeyed in fully-developed flows where the diffusion flux for all flow variables in the exit direction is zero.
- **Walls**:

Bottom wall: Heated (constant temperature, $T=Th$).
Top wall: Cooled ($T=Tc$).

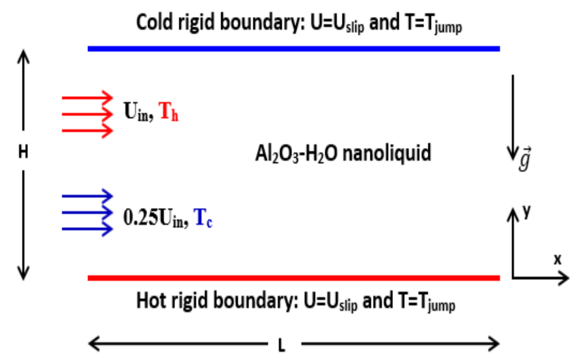

Figure 1. Schematic of the physical model of the microchannel.

Effect of geometric ratio (H/L):

- **A smaller H/L** (longer channel) promotes fully de–veloped flow, reducing entrance effects but inc–reasing viscous losses.
- **A larger H/L** (shorter channel) enhances entrance region effects, potentially improving Nu at the cost of higher pressure drop.

The study likely assumes fixed **H/L**; parametric analysis of this ratio could be future work and is of interest in literature ([29]).

3. ASSUMPTIONS & BOUNDARY CONDITIONS

Key Assumptions

- Laminar, incompressible flow (*Re* ≤ 50, valid for microscale flows).
- Slip flow regime (0.001 < *Kn* < 0.1): Velocity slip/temperature jump at walls.
- Negligible radiation/gravity effects: Dominated by forced convection.
- Newtonian nanofluid: Homogeneous dispersion of nanoparticles (no aggregation).
- Thermophysical properties: Constant except for density (Boussinesq approximation if buoyancy is considered).

Initial & boundary conditions

- **Flow**:

Inlet:
$H/2 \le Y \le H$: $U=U_{in}$, $T=T_h=1$
$0 \le Y \le H/2$: $U=0.25U_{in}$, $T=T_c=0$
Outlet: (fully developed flow).

$$\frac{\partial U}{\partial Y}=\frac{\partial V}{\partial Y}=\frac{\partial T}{\partial Y}$$

- **Walls**:

Near the horizontal walls, the modeling of the flow and heat transfer need to apply the slip velocity and temperature jump conditions in its dimensional forms [27, 5, 19]):

$$u^{slip}_{y=0}=u_{x,y=0}-u_{x,paroi}=\sigma\,\mathrm{Kn}\left(\frac{\partial u}{\partial y}\right)_{y=0} \tag{1}$$

$$u^{slip}_{y=H}=u_{x,paroi}-u_{x,y=H}=\sigma\,\mathrm{Kn}\left(\frac{\partial u}{\partial y}\right)_{y=H} \tag{2}$$

$$\begin{aligned}T^{jump}_{x,y=0}&=T_{x,y=0}-T_{x,paroi}\\&=\zeta\,\mathrm{Kn}\left(\frac{2\gamma}{(\gamma+1)\mathrm{Pr}}\right)\left(\frac{\partial T}{\partial y}\right)_{y=0}\end{aligned} \tag{3}$$

$$\begin{aligned}T^{jump}_{x,y=H}&=T_{x,paroi}-T_{x\,y=H}\\&=\zeta\,\mathrm{Kn}\left(\frac{2\gamma}{(\gamma+1)\mathrm{Pr}}\right)\left(\frac{\partial T}{\partial y}\right)_{y=H}\end{aligned} \tag{4}$$

σ, ξ , γ, Kn, and Pr are respectively, the tangential momentum accommodation coefficient, the thermal accommodation coefficient, the specific heat transfer ratio, the Knudsen number, and the Prandtl number.

Governing equations

The flow and heat transfer of the co-flow through the micro-channel is governed by the incompressible Navier Stokes coupled with the energy equations [30].

Continuity equation:

$$\frac{\partial U}{\partial X}+\frac{\partial V}{\partial Y}=0 \tag{5}$$

Momentum equations:

$$U\frac{\partial U}{\partial X}+V\frac{\partial U}{\partial Y}=-\frac{\partial P}{\partial X}+\frac{\mu_{nf}}{\rho_{nf}\upsilon_f}\frac{1}{\mathrm{Re}}\left(\frac{\partial^2 U}{\partial X^2}+\frac{\partial^2 U}{\partial Y^2}\right) \tag{6}$$

$$U\frac{\partial V}{\partial X}+V\frac{\partial V}{\partial Y}=-\frac{\partial P}{\partial Y}+\frac{\mu_{nf}}{\rho_{nf}\upsilon_f}\frac{1}{\mathrm{Re}}\left(\frac{\partial^2 V}{\partial X^2}+\frac{\partial^2 V}{\partial Y^2}\right) \tag{7}$$

Energy equation:

$$U\frac{\partial \theta}{\partial X}+V\frac{\partial \theta}{\partial Y}=\frac{\alpha_{nf}}{\alpha_f}\frac{1}{\mathrm{Re}\,\mathrm{Pr}}\left(\frac{\partial^2 \theta}{\partial X^2}+\frac{\partial^2 \theta}{\partial Y^2}\right) \tag{8}$$

The local irreversibility inside the micro-heat-exchanger is subdivided into two terms: the first corresponds to the heat transfer irreversibility (S_θ) and the second corresponds to the fluid friction irreversibility (S_f) [20,21,31–33].

$$S\_gen-local = S_\theta + S_f \tag{9}$$

$$S\_gen-local = \left\{ \frac{\partial^2\theta}{\partial X^2} + \frac{\partial^2\theta}{\partial Y^2} \right\} + \zeta_1 \left\{ 2\left[\left(\frac{\partial U}{\partial X}\right)^2 + \left(\frac{\partial V}{\partial Y}\right)^2 \right] + \left(\frac{\partial U}{\partial Y} + \frac{\partial V}{\partial X} \right)^2 \right\} \tag{10}$$

The local Bejan number is expressed in Eq. (11):

$$Be\_local = HTI / S\_gen-local \tag{11}$$

The irreversibility distribution ratio, which equals 10^{-5} in this study is expressed as:

$$\zeta_1 = \frac{\mu_{hnf} T_0}{k} \left(\frac{\alpha}{H \Delta T} \right)^2 \tag{12}$$

The average entropy generation and Be number are expressed in Eqs. (13) and (14):

$$S\_gen = \iint_\Omega S\_gen-local \; dXdY \tag{13}$$

$$Be = \iint_\Omega Be\_local \; dXdY \tag{14}$$

The local Nusselt number, calculated along the bottom wall as shown below, determines the microflow's heat transfer characteristics.

$$Nu_{local} = -\frac{k_{nf}}{k_f} \left(\frac{\partial T}{\partial Y} \right)_{X=0} \tag{15}$$

Therefore, the average Nusselt number is obtained by integrating the local Nusselt number.

$$Nu\_avg = -\frac{1}{L} \frac{k_{nf}}{k_f} \int_0^L \left(\frac{\partial T}{\partial Y} \right)_{X=0} \tag{16}$$

4. NUMERICAL MODELING

The Lattice Boltzmann method is used with the D_2Q_9 model (Figure 2) for solving both motion and energy equations in micro-heat-exchanger.

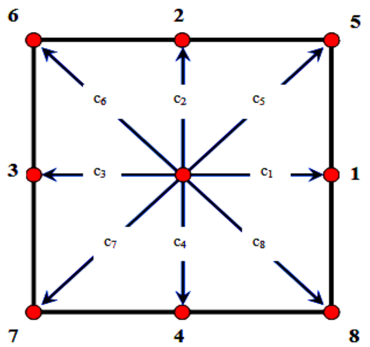

Figure 2. The D_2Q_9 LBM model.

This model is validated in previous investigations for cases of macro [34] and micro geometry [22,28]. The lattice Boltzmann method has been used successfully in various classic and emerging scientific and engineering fields and has proven powerful to pose an alternative to classical discretization methods in the continuous and slip regimes.

4.1 Lattice Boltzmann equation

The double-population method enhances the accuracy of the model, particularly in capturing the finer details of the near-wall flow and heat transfer.

$$f_k(x + c_k \Delta t, t + \Delta t) = f_k(x,t) + \frac{\Delta t}{\tau_\nu} \left[f_k^{eq}(x,t) - f_k(x,t) \right] + \Delta t F_k \tag{7}$$

$$g_k(x + c_k \Delta t, t + \Delta t) = g_k(x,t) + \frac{\Delta t}{\tau_\alpha} \left[g_k^{eq}(x,t) - g_k(x,t) \right] \tag{8}$$

Equations (20) and (21) contain single relaxation times, which are related to the kinematic viscosity and the thermal diffusivity via Equation (22):

$$\tau_\upsilon = 3\upsilon \frac{\Delta t}{\Delta x^2} + 0.5, \;\; \tau_\alpha = 3\alpha \frac{\Delta t}{\Delta x^2} + 0.5 \tag{19}$$

The equilibrium distribution functions corresponding to the medium are calculated as follows:

$$f_i^{eq} = \omega_k \rho \left(1 + 3 \frac{c_k u}{c_s^2} + \frac{9}{2} \frac{(c_k u)^2}{c_s^4} - \frac{3}{2} \frac{(u)^2}{c_s^2} \right) \tag{20}$$

For thermal simulation the equilibrium distribution function is calculated as follows:

$$g_i^{eq} = T \omega_k \left(1 + 3 \frac{c_k u}{c_s^2} \right) \tag{21}$$

The speed of sound Eq. (22) and the lattice weight factors ω_k Eq. (23) are expressed as follows:

$$c_s = c_k / \sqrt{3} \tag{22}$$

$$\omega_{k=0} = \frac{4}{9}, \;\; \omega_{k=1-4} = \frac{1}{9}, \;\; \omega_{k=5-8} = \frac{1}{36} \tag{23}$$

Macroscopic properties (density, velocity, temperature) are calculated at nodal points throughout the domain.

$$\rho(x,t) = \sum_0^8 f_k, \; \rho(x,t) u_k(x,t) = \sum_0^8 f_k \; c_k + \frac{\Delta t}{2} F_k \qquad T(x,t) = \sum_0^8 g_k \tag{24}$$

4.2 Hydrodynamic boundary conditions

- At the inlet:

The unknown distribution functions are calculated using the boundary condition proposed by Zou and He [35].

- At the outlet:
  A second-order extrapolation scheme is used [36].
- Side walls:
  The slip velocity condition is applied to the horizontal walls [22,37,38]:

4.3 Thermal boundary conditions

- At the inlet:

$$g_1 = T_{inlet}\left(\omega(1)+\omega(3)\right)-g_3 \tag{25}$$

$$g_5 = T_{inlet}\left(\omega(5)+\omega(7)\right)-g_7 \tag{26}$$

$$g_8 = T_{inlet}\left(\omega(6)+\omega(8)\right)-g_6 \tag{27}$$

- Side walls:
  The temperature jump condition is applied to the horizontal wall [22,37,38].
- At the outlet, an extrapolation scheme is used [39]:

$$g_3(x_w,j) = 2\times g_3(x_w-1,j)-g_3(x_w-2,j) \tag{28}$$

$$g_6(x_w,j) = 2\times g_6(x_w-1,j)-g_6(x_w-2,j) \tag{29}$$

$$g_7(x_w,j) = 2\times g_7(x_w-1,j)-g_7(x_w-2,j) \tag{30}$$

5. JUSTIFICATION OF MODEL CHOICES

- LBM: Captures microscale effects since the mesoscopic approach (slip flow, Knudsen layers) is better than traditional CFD.
- RSM: Efficiently maps nonlinear interactions between *Re, Kn, Vf, Dp*.
- Neglected effects: Turbulence (low *Re*), particle sedimentation (assumed stable nanofluid).

However, we may suggest improvements in future works to the limitations of the present study:

- *H/L* ratio and its impact.
- Manufacturing feasibility (e.g., microfabrication limits for *Dp* = 10 nm).
- 3D effects (e.g., sidewall conduction) are negligi–ble.

6. NUMERICAL VALIDATION

Firstly:

The case of a two-dimensional heated macro channel crossed with cold air (Pr=0.71) was taken as a bench–mark test in order to ensure that the obtained results were correct. The channel was heated from its top and bottom walls. The velocity profile at different sections of the channel is compared with those obtained by Tang *et al.* [40] and Mohebbi *et al.* [41] (Figure 3a). Based on the aforementioned comparisons, the present results show a good agreement. In addition, the fully developed velocity is compared to the analytical solution (U_{max} = U_{in}= 1.5) (Figure 3 b).

The analytical solution for fully-developed flow between two parallel plates is defined as [42].

$$\frac{u}{u_{in}} = \frac{3}{2}\left(\frac{4y}{H}-\left(\frac{2y}{H}\right)^2\right) \tag{31}$$

The results agree with the analytical one. Besides, LBM findings are highly accurate.

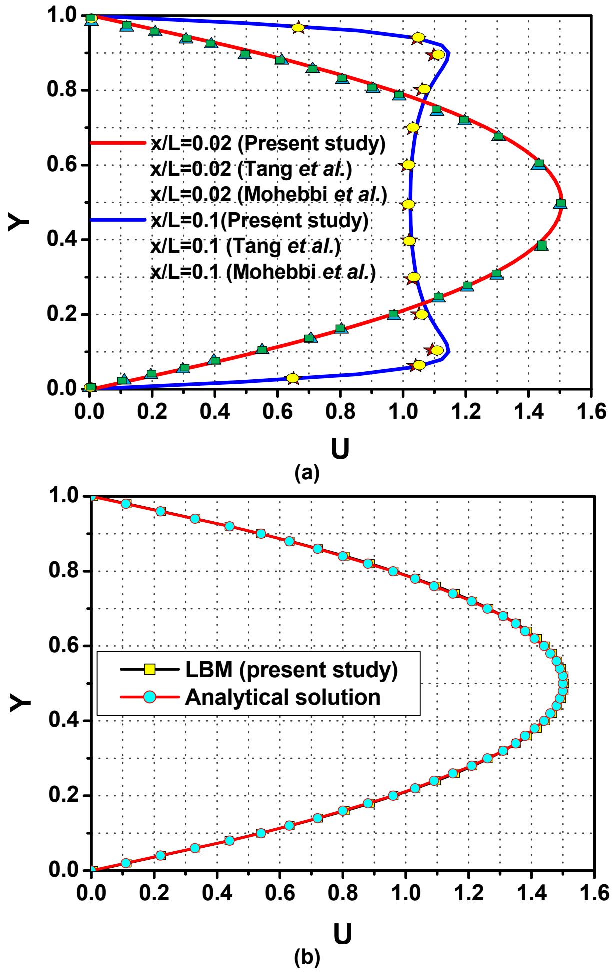

Figure 3. (a) Velocity profiles at various channel sections compared against results by Tang *et al.* [40] and Mohebbi *et al.* [41]; (b) Fully-developed velocity profile validated against the analytical exact solution.

Secondly:

To validate the accuracy of the developed FORTRAN code, Figure 4 compares the fully deve–loped horizontal velocity profiles across a microchannel partially heated from side walls filled with Cu-water nanofluid at various Knudsen numbers (Kn) with results from Ferhi et al. [22]. Excellent agreement is observed.

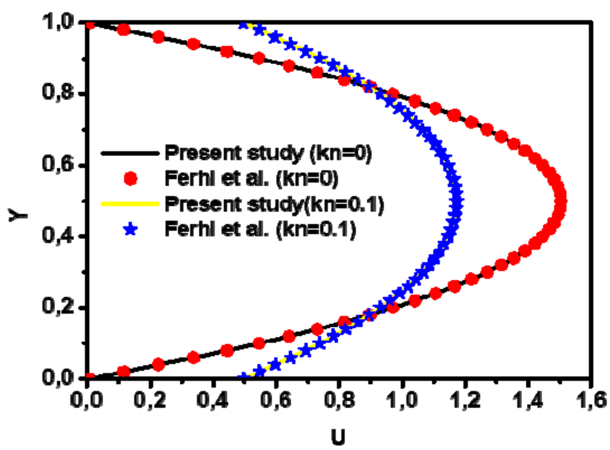

Figure 4. Fully developed horizontal velocity profiles for Re=50: Present results compared with Ref. [22].

Thirdly:

A microchannel partially heated from side walls filled with Cu-water nanofluid was simulated using the

Lattice Boltzmann Method (LBM). The model's accu–racy was validated by comparing its predictions against established models for a range of Reynolds numbers (*Re*). The results, summarized in Table 1, demonstrated sufficient agreement across all tested Re values, thereby establishing confidence in the LBM model's ability to accurately simulate heat transfer in this complex system.

Table 1. Comparison of the present results with those obtained in the literature for the case of two-dimensional microchannel partially heated from side walls filled with nanofluid for *Kn*=0.1.

	Re					
	10		50		100	
(Nu_avg)	Present	Ref. [22]	Present	Ref. [22]	Present	Ref. [22]
	14.93	14.93	28.58	28.58	38.18	38.18

7. RESULTS AND DISCUSSION

In this section, the impact of several independent emer–ging parameters on thermodynamic characteristics and the entropy generation of a co-flow crossed the micro-heat-exchanger. Besides, the response of heat transfer and volumetric entropy generation is determined based on the interaction between several designs' parameters and then an optimized model is obtained using response surface methodology.

7.1. Independent impact of design monitoring factors

Convective flow: The impact of each important design parameter such as *Kn* and *Re* on the developed velocity, slip velocity, and temperature jump is illustrated in Figures 5 and 6 respectively.

As the *Kn* number rises, the movement of the particles in the core region of the micro-heat-exchanger becomes decelerated. On the other hand, near the side walls, the velocity increases. This can be explained by the collision between particles-particles and particles-walls which are more important near the bottom and top side walls (Figure 5). Indeed, the velocity profile established in the micro-heat-exchanger is greatly affected by the Reynolds number (*Re*) and the Knudsen number (*Kn*). At low Re (laminar flow), the velocity profile usually appears parabolic, featuring a peak velocity at the center of the micro-channel and no velocity at the walls owing to the no-slip condition. The Knudsen number (*Kn*), which denotes the ratio of the average free path of fluid molecules to the characteristic length of the micro-channel, gains significance as the micro-channel dimensions decrease. When *Kn* rises (slip flow regime), the no-slip boundary condition ceases to hold, leading to a non-zero velocity. Consequently, the slip velocity and the temperature jump increase (Figure 6a and b). As the Re number increases, the convective motion increases which reduces the hydrodynamic boundary and the thermal layer thickness.

Heat transfer and entropy generation: The variation of heat transfer and entropy generation as a function of Re and *Kn* are illustrated in Figure 7. It can be seen from this figure that the heat transfer rate's (Figure 7a) dependence on the Reynolds number follows a positive trend, meaning higher Re leads to higher heat transfer rates. However, the specific relationship is highly dependent on the convective flow intensity. As Re increases convective heat transfer becomes increasingly dominant, leading to a stronger dependence on the heat transfer rate on Re. Moreover, the variation of entropy generation (Figure 7b) with Reynolds number in a co-flow through a micro-channel depends on the interplay between fluid friction and energy irreversibility. At low Re, viscous dissipation is minimal, and entropy generation is primarily driven by energy irreversibility, potentially exhibiting a weak dependence on *Re*. As *Re* increases, fluid friction increases significantly, leading to a substantial rise in entropy generation due to viscous dissipation. However, enhanced heat transfer at higher Re can, in some cases, partially offset this increase. While *Nu_avg* rises linearly with Re (Figure 7a), *S_gen* surges due to viscous dissipation (Figure 7b). This confirms that high Re improves heat transfer at the cost of irreversibility.

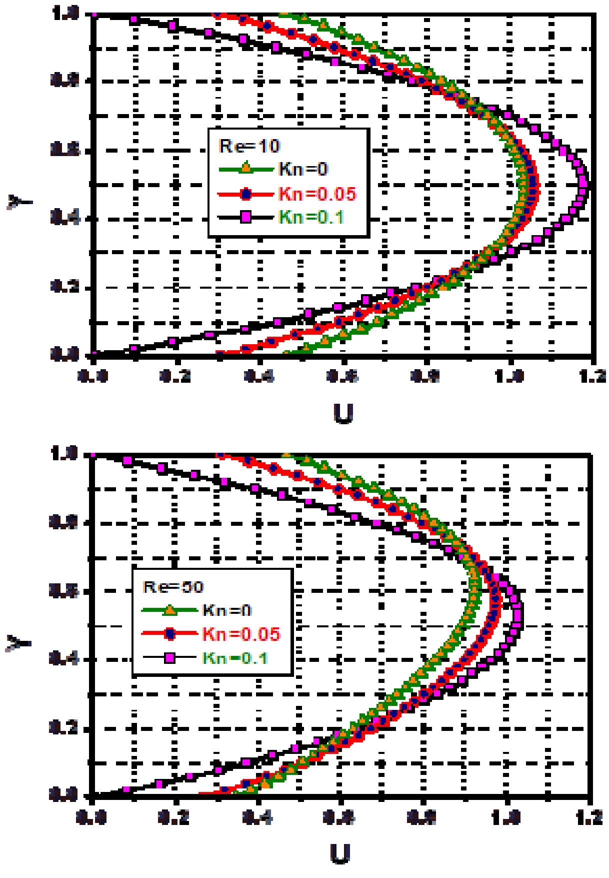

Figure 5. Developed velocity inside the micro-heat-exchanger for different *Re* and *Kn*.

In addition, the heat transfer rate in a co-flow through a micro-channel exhibits a complex relationship with the Knudsen number (*Kn*), reflecting the transition from continuum to rarefied flow. At low *Kn* (continuum regime), the heat transfer is primarily governed by convection and conduction. As *Kn* increases, rarefaction effects become significant. Slip flow at the walls alters the velocity and temperature profiles, influencing both convective and conductive heat transfer. Thermal slip, in particular, leads to a reduced temperature gradient near the walls, potentially decreasing the conductive heat transfer. The overall effect on the heat transfer rate depends on the relative contributions of these competing mechanisms. For sufficiently high Kn (free molecular flow), the heat transfer becomes dominated by molecular collisions with the walls, leading to an increase in the heat transfer, particularly at high Re. Higher *Kn* (slip flow) reduces *S_gen* by lowering shear stress but can dampen *Nu_avg* if thermal slip dominates (Figure 7). Thus, *Kn*=0.1 offers a trade-off-moderate *Nu_avg* with minimal *S_gen*.

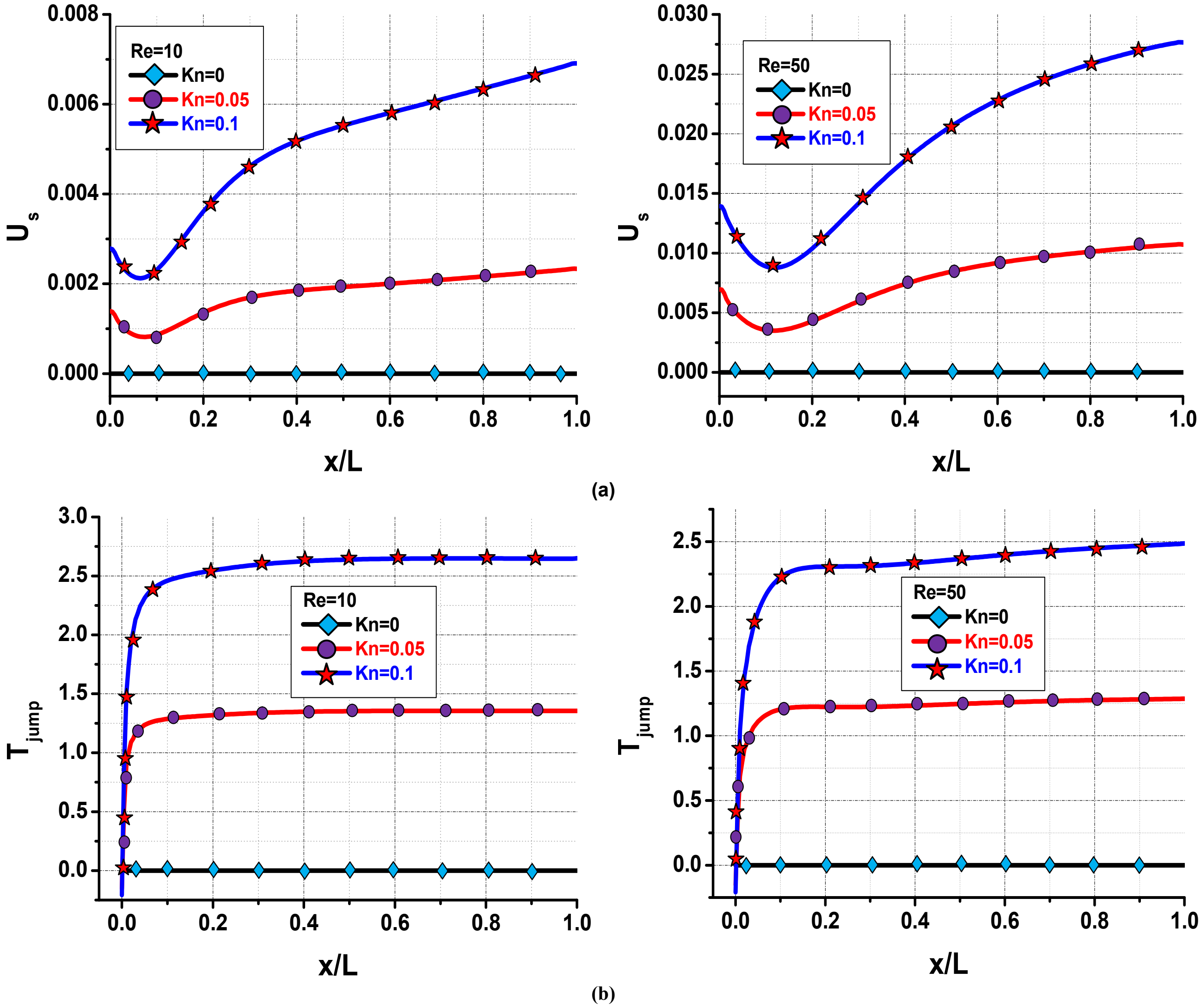

Figure 6. Slip velocity (a) and temperature jump (b) along the bottom side wall.

On the other hand, the variation of entropy generation with Knudsen number in a co-flow through a micro-channel is primarily influenced by the transition from continuum to slip flow regimes. At low *Kn*, the entropy generation is primarily governed by viscous dissipation and irreversibility. As *Kn* increases (approaching the slip flow regime), the no-slip boundary condition becomes invalid, and slip velocities at the micro-channel walls alter the velocity profile and shear stress distribution. This modification affects viscous dissipation and consequently the entropy generation due to friction. Simultaneously, the heat transfer characteristics change due to the altered velocity profile and thermal slip, influencing the irreversibility. Therefore, the entropy generation reduction depends on the relative contribution of viscous dissipation and irreversibility, which are both affected by the degree of rarefaction characterized by *Kn*.

7.2 Optimization process using Response surface methodology

RSM is a collection of statistical and mathematical techniques used for modeling and analyzing problems in which a response of interest is influenced by several factors. The goal is to optimize the response. Usually, in the beginning stages of an experiment, the factors influencing the response are not well understood.

RSM helps in understanding the relationship between the factors and the response by providing a sequential experimental strategy. RSM uses a set of designed experiments to obtain an adequate description of the response surface. Based on this descriptive model, one can find operating conditions for the factors that yield a desired improvement in the response. The sequential approach consists of three steps:

- The first step is to conduct a screening experiment to identify the most important factors (*Re, Kn, Vf,* and *Dp*) gathered in Table 2.
- The second step is to conduct experiments on the factors identified in the first step to develop and fit a model for the response (response of *Nu_avg* and *S_gen* illustrated in Table 3).
- The final step is to conduct experiments to find the optimal settings for the factors.

RSM has several advantages compared to other data analysis techniques used in the optimization process. First, a small number of experiments can produce adequate data to optimize the product or process. Also, the underlying statistical model gives the user clear information about the adequacy of the data. Additionally, it is a suitable method in the optimization process for developing new products, process optimization, and efficiency improvement of established processes.

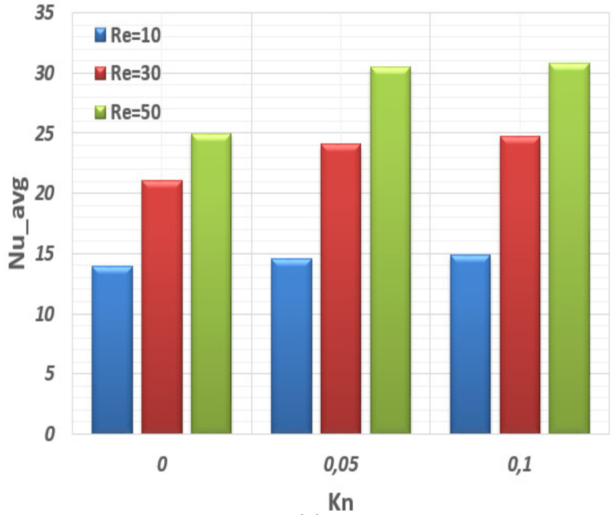

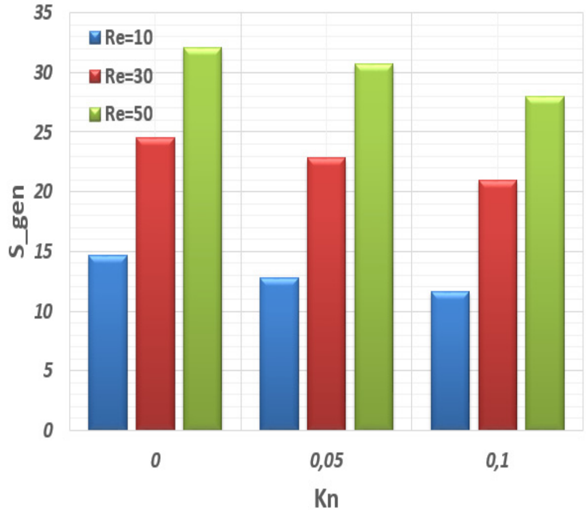

Figure 7. Impact of *Re* and *Kn* on heat transfer *Nu_avg* (a) and entropy generation *S_gen* (b).

Table 2. The effective factors studied and the values on three levels

Actual symbol	Effective factor	Level		
		Low (-1)	Medium (0)	High (+1)
A: Re	Reynolds number	10	30	50
B: V_f	Volume fraction	0	0.02	0.04
C: Kn	Knudsen number	0	0.05	0.1
D: Dp (nm)	Nanoparticles size			

Table 3. Design of Experiments and response of *Nu_avg* and *S_gen*.

	Input design factors				Responses	
Runs	***Re***	***V_f***	***Kn***	***Dp (nm)***	***Nu_avg***	***S_gen***
1	10	0.02	0.00	30	12.43	14.85
2	50	0.02	0.00	30	21.75	32.51
3	10	0.02	0.1	30	13.01	11.81
4	50	0.02	0.1	30	27.52	28.44
5	30	0.00	0.05	10	18.11	23.48
6	30	0.04	0.05	10	30.62	18.02
7	30	0.00	0.05	50	18.06	23.46
8	30	0.04	0.05	50	22.66	24.33
9	10	0.02	0.05	10	15.03	11.67
10	50	0.02	0.05	10	30.94	26.99
11	10	0.02	0.05	50	12.89	13.47
12	50	0.02	0.05	50	25.55	32.13
13	30	0.00	0.00	30	15.77	25.27
14	30	0.00	0.1	30	18.68	21.58
15	30	0.04	0.00	30	20.43	24.56
16	30	0.04	0.1	30	24.70	20.98
17	10	0.00	0.05	30	11.15	13.11
18	50	0.00	0.05	30	22.64	31.43
19	10	0.04	0.05	30	14.55	12.75
20	50	0.04	0.05	30	30.51	30.71
21	30	0.02	0.00	10	21.49	21.59
22	30	0.02	0.1	10	24.97	18.42
23	30	0.02	0.00	50	17.64	25.81
24	30	0.02	0.1	50	20.93	22.03
25	30	0.02	0.05	30	21.05	23.18

Interaction effect on 3D response surface of *Nu_avg* and *S_gen*: The impact of the interaction between the input monitoring factors on the response of energy transfer rate (*Nu_avg*) is depicted in Figure 8. By analyzing the response surface of heat transfer, this last depends linearly as a function of *Vf* and *Re*. On the other hand, the heat transfer undergoes a nonlinear curve versus *Kn* and *Dp*. The Nu improvement is more pronounced for high values of *Re, Kn*, and volume fraction (*Vf*) and for low values of nanoparticle diameter (*Dp*). Moreover, Raising Re typically boosts Nu_avg because of heightened turbulence and mixing; however, this impact is usually more subdued in micro-channels than in macro-channels because of the prevalence of viscous forces. Increased nanoparticle volume fractions (*Vf*) generally result in higher *Nu_avg* because of the improved thermal conductivity of the nanofluid. Nonetheless, this improvement is not consistently linear and can be affected by the aggregation of nanoparticles and the Brownian movement. Typically, smaller nanoparticle diameters (*Dp*) lead to higher *Nu_avg* because they offer a greater surface area for heat transfer and enhanced dispersion in the base fluid.

Ultimately, the Knudsen number (*Kn*), which is the ratio of the average free path of fluid molecules to the hydraulic diameter of the channel, is crucial in microchannels. As *Kn* increases (nearing the slip flow regime), the no-slip boundary condition fails, resulting in variations from traditional correlations and possibly influencing the connection between *Nu_avg* and the other variables. As a result, the fluctuation of *Nu_avg* is a complex interaction of these elements, and precise forecasting necessitates taking their combined impacts into account via advanced modeling methods that inco-rporate micro-scale. The case of a high heat transfer rate can be used in many industrial applications.

The impact of the interaction between the input monitoring factors on the response of thermodynamic irreversibility (*S_gen*) is illustrated in Figure 9. To obtain the optimized model, the volumetric entropy generation must be the minimum possible. By analyzing the response surface of entropy generation, it is found that the minimum entropy generation occurs at high Knudsen number (*Kn*), low values of nanoparticle diameter (*Dp*), and high nanoparticle volume fraction (*Vf*). In addition, increasing Re leads to higher entropy generation due to increased fluid friction and viscous dissipation. However, the relationship isn't always linear, and the effect might be less pronounced in mic–rochannels where viscous effects are dominant. Higher nanoparticle volume fractions (*Vf*) can increase entropy generation due to enhanced viscous dissipation from increased fluid viscosity and potentially from irre–versible processes associated with nanoparticle aggre–gation and Brownian motion. Smaller nanoparticle diameters (*Dp*) might initially reduce entropy generation by improving heat transfer, but this effect can be coun–teracted by increased viscous dissipation if the smaller particles lead to a significant increase in viscosity.

The *Kn* number plays a crucial role in the slip flow regime. As *Kn* increases, the deviations from the no-slip condition can affect both fluid friction and heat transfer, thus altering the overall entropy generation. Therefore, the variation of entropy generation is a complex inter–play of these parameters, with the optimal conditions for minimizing entropy generation often representing a trade-off between enhancing heat transfer and reducing viscous dissipation. Accurate prediction requires consi–dering the combined and often non-linear effects of these factors through detailed numerical simulations or advanced analytical models.

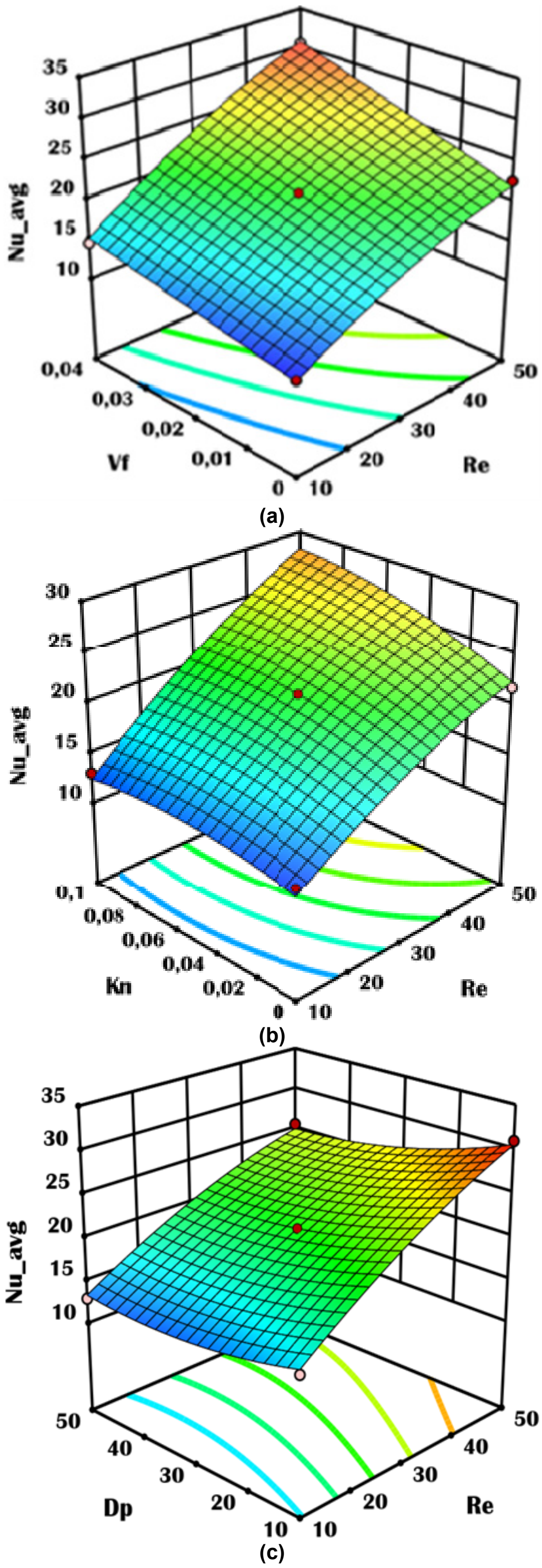

Figure 8. 3D response surface for *Nu_avg* showing interactions between (a) *Re* and *Vf*, (b) *Re* and *Kn*, and (c) *Vf* and *Dp*.

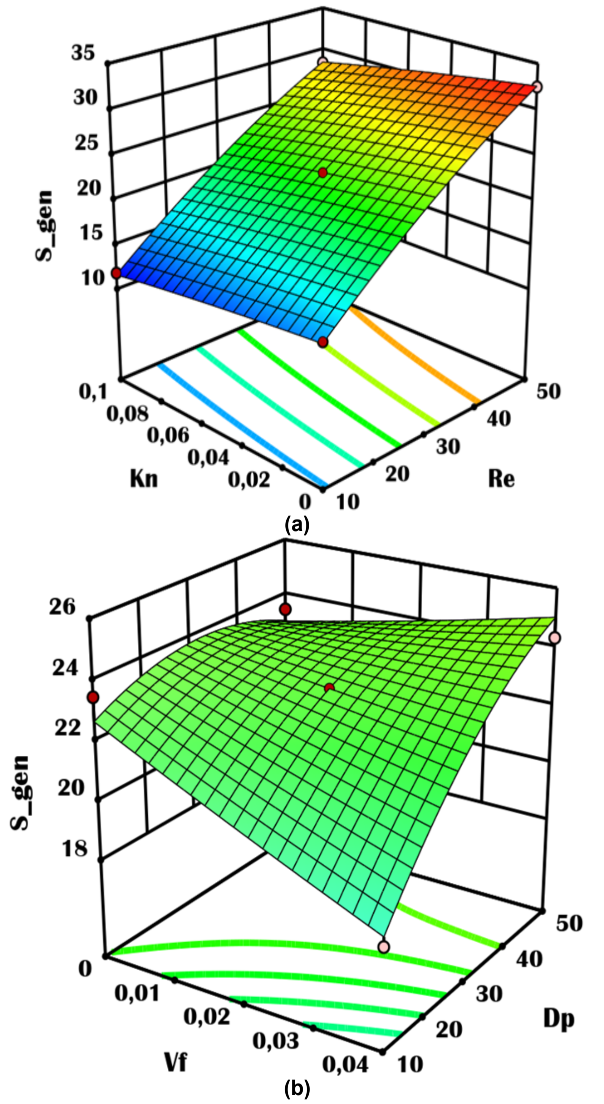

Figure 9. 3D response surface for *S_gen* highlighting (a) *Re-Kn* trade-offs and (b) *Vf-Dp* effects.

Analysis of variance (ANOVA): Analysis of variance (ANOVA for quadratic model) is a statistical technique employed to assess the importance level of the model or input factors, suggest a regression model relating the input variables to the objective function, and assess the accuracy of the regression model. The input variable or model variables are deemed significant or insignificant based on P or F values. In this study, 0.05 and 1 are established as the critical significance levels for P and F, respectively. Typically, the most important model has the lowest P-value and the highest F-value. It is observed from Table 4 that the P values for *AD, BC, CD,* A^2, B^2, *and* C^2 are greater than 0.05, suggesting that these terms are not significant model terms for deter–mining *Nu_avg*. The Model F-value of 60.42 suggests that the model is significant. There is merely a 0.01% likelihood that such a large F-value could result from random noise. P-values below 0.05 suggest that the model terms are significant. In this scenario, A, B, *C, D, AB, AC, BD,* and D^2 are important model components. Values exceeding 0.1 suggest that the model terms lack significance. Having numerous insignificant model ter–ms may lead to an enhancement of our model through model reduction.

It is observed from Table 5 that the P values for *AB, AC, BC, CD,* B^2, and C^2 are greater than 0.05, sugges–ting that these terms are not significant model terms for determining S_gen. The Model F-value of 233.88 suggests that the model is significant. There is merely a 0.01% likelihood that such a large F-value could result from random noise. P-values below 0.05 suggest that the model terms are significant. In this scenario, *A, B, C, D, AD, BD,* A^2, and D^2 are important model compo–nents. Values exceeding 0.1 suggest that the model terms lack significance. Having numerous insignificant model terms may lead to an enhancement of our model through model reduction. The developed polynomial models for *Nu_avg* and *S_gen* in terms of actual design factors are written in Eqs. 35 and 36.

Additionally, the normal probability plots for both the *Nu_avg* and *S_gen* residuals are shown in Figure 10, revealing a straight line, which signifies that the model is effective, and the errors follow normal distributions. Residual points uniformly spread around the straight line on these probability plots exhibit the traits of a sui–table model. In line with the appropriate model, verifi–cation was additionally examined through regression analysis to confirm that the model accurately reflects the real data. The residuals in relation to the predicted va–lues for heat transfer rate and entropy generation shown in Figure 11 suggest that the model is sufficient. This figure displayed the graphs of predicted versus actual values for *Nu_avg* and *S_gen*, allowing for the analysis of the correlation between them based on the model's quadratic equation. The successful correlation with the linear regression is evident in these graphs (the R^2 values of 0.9883 and 0.997 for *Nu_avg* and *S_gen* respectively), thus highlighting the model's precision in representing the data points.

$$Nu\_avg = 7.11896 + 0.464896 \times Re + 214.37500 \times Vf + 33.98333 \times Kn - 0.135687 \times Dp \\ + 1.2975 \times Re \times Kn - 4.94375 \times Vf \times Dp + 0.003338 \times Dp^2 \tag{34}$$

$$S\_gen = 8.45219 + 0.565063 \times \mathrm{Re} - 148.5625 \times Vf - 17.11667 \times Kn + 0.099625 \times Dp \\ + 0.002088 \times \mathrm{Re} \times Dp + 3.95625 \times Vf \times Dp - 0.002911 \times \mathrm{Re}^2 - 0.002433 \times Dp^2 \tag{35}$$

Table 4: ANOVA for a quadratic model of *Nu_avg*.

Source	Sum of Squares	df	Mean Square	F-value	p-value	
Model	804.18	14	57.44	60.42	**< 0.0001**	significant
A-Re	531.34	1	531.34	558.85	< **0.0001**	significant
B-Vf	127.14	1	127.14	133.72	< **0.0001**	significant
C-Kn	34.34	1	34.34	36.12	**0.0001**	significant
D-Dp	45.75	1	45.75	48.12	< **0.0001**	significant

(nm)						
AB	5.00	1	5.00	5.25	**0.0449**	significant
AC	6.73	1	6.73	7.08	**0.0238**	significant
AD	2.64	1	2.64	2.78	0.1266	
BC	0.4624	1	0.4624	0.4863	0.5015	
BD	15.64	1	15.64	16.45	**0.0023**	significant
CD	0.0090	1	0.0090	0.0095	0.9243	
A²	4.63	1	4.63	4.87	0.0519	
B²	0.0048	1	0.0048	0.0051	0.9447	
C²	3.49	1	3.49	3.67	0.0845	
D²	5.03	1	5.03	5.29	**0.0442**	significant

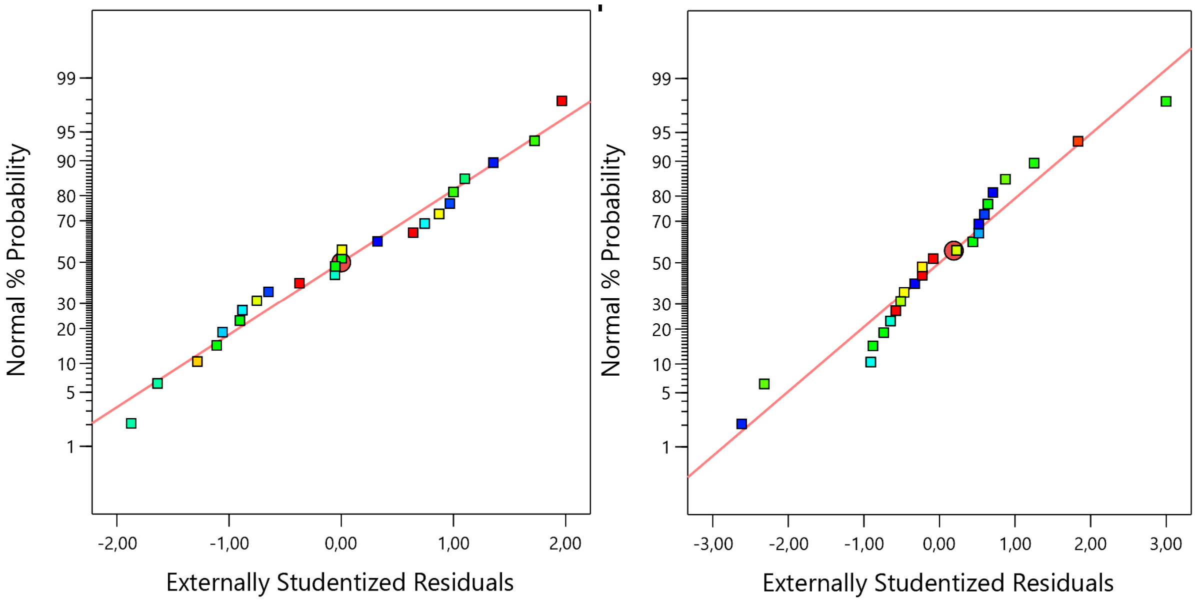

Figure 10. Normal probability plot of *Nu_avg* (left) and *S_gen* (right).

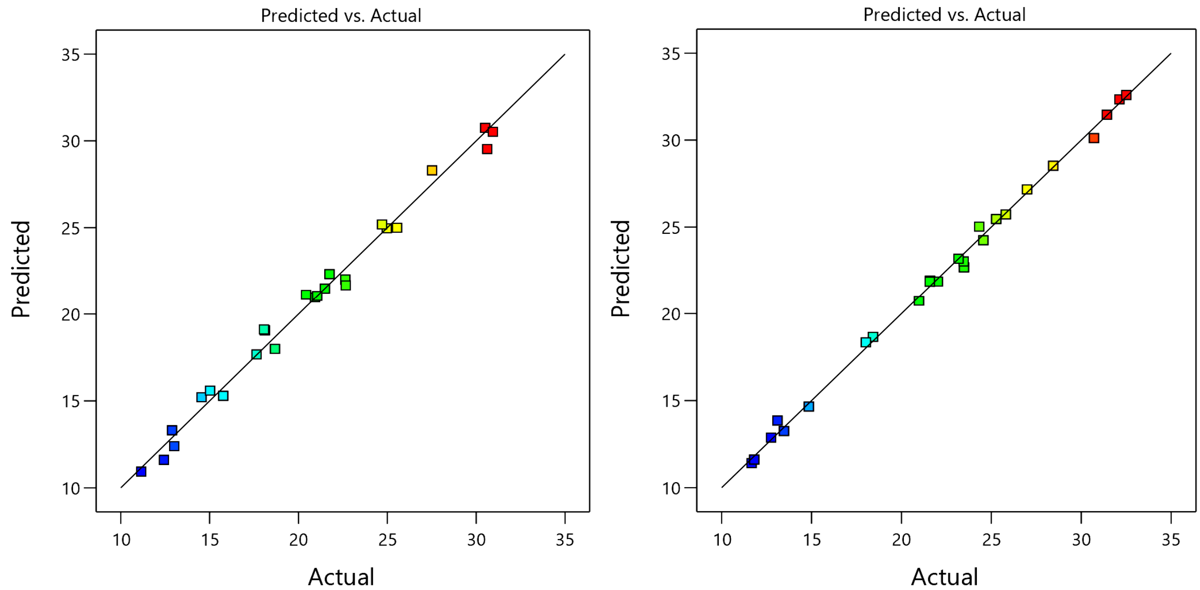

Figure 11. Plots of regression quality between actual and predicted values of *Nu_avg* (left) and *S_gen* (right).

Table 5: ANOVA for a quadratic model of *S_gen*.

Source	Sum of Squares	df	Mean Square	F-value	p-value	
Model	1012.85	14	72.35	233.88	**< 0.0001**	significant
A-Re	910.89	1	910.89	2944.70	**< 0.0001**	significant
B-Vf	4.06	1	4.06	13.13	**0.0047**	significant
C-Kn	37.91	1	37.91	122.57	**< 0.0001**	significant
D-Dp (nm)	36.96	1	36.96	119.48	**< 0.0001**	significant
AB	0.0324	1	0.0324	0.1047	0.7529	

AC	0.2652	1	0.2652	0.8574	0.3763	
AD	2.79	1	2.79	9.02	**0.0133**	significant
BC	0.0030	1	0.0030	0.0098	0.9232	
BD	10.02	1	10.02	32.38	**0.0002**	significant
CD	0.0930	1	0.0930	0.3007	0.5955	
A^2	3.83	1	3.83	12.38	**0.0056**	significant
B^2	0.0107	1	0.0107	0.0347	0.8559	
C^2	0.0788	1	0.0788	0.2548	0.6246	
D^2	2.67	1	2.67	8.65	**0.0148**	significant

***Optimal monitoring parameters*:** The interaction between the controlling design parameters of the current micro-heat-exchanger leads to obtaining an optimized configuration with a maximum value of heat transfer close to 30.8387 and a minimum of volumetric entropy production equal to 16.845. The optimized configura–tion corresponds to *Re* = 30.7, *Kn* = 0.1, *Vf* = 0.04, and *Dp* = 10. The optimum (*Re* = 30.7, *Kn* = 0.1, *Vf* = 0.04, *Dp* = 10) does not maximize Nu (which peaks at *Re*=50) but achieves 85% of peak *Nu_avg* with 40% lower *S_gen* compared to *Re* =50.

While RSM identifies a parameter set (*Re*=30.7, *Kn*=0.1, *Vf*=0.04, *Dp*=10) that balances *Nu_avg* and *S_gen*, true simultaneous optimization is unattainable. For instance:

- Max *Nu_avg* (*Re*=50, *Vf*=0.04) → High *S_gen* (Table 2, Run 2).
- Min *S_gen* (*Re*=10, *Kn*=0.1) → Low *Nu_avg* (Table 2, Run 3).

Thus, the optimum is a practical compromise for energy-efficient systems.

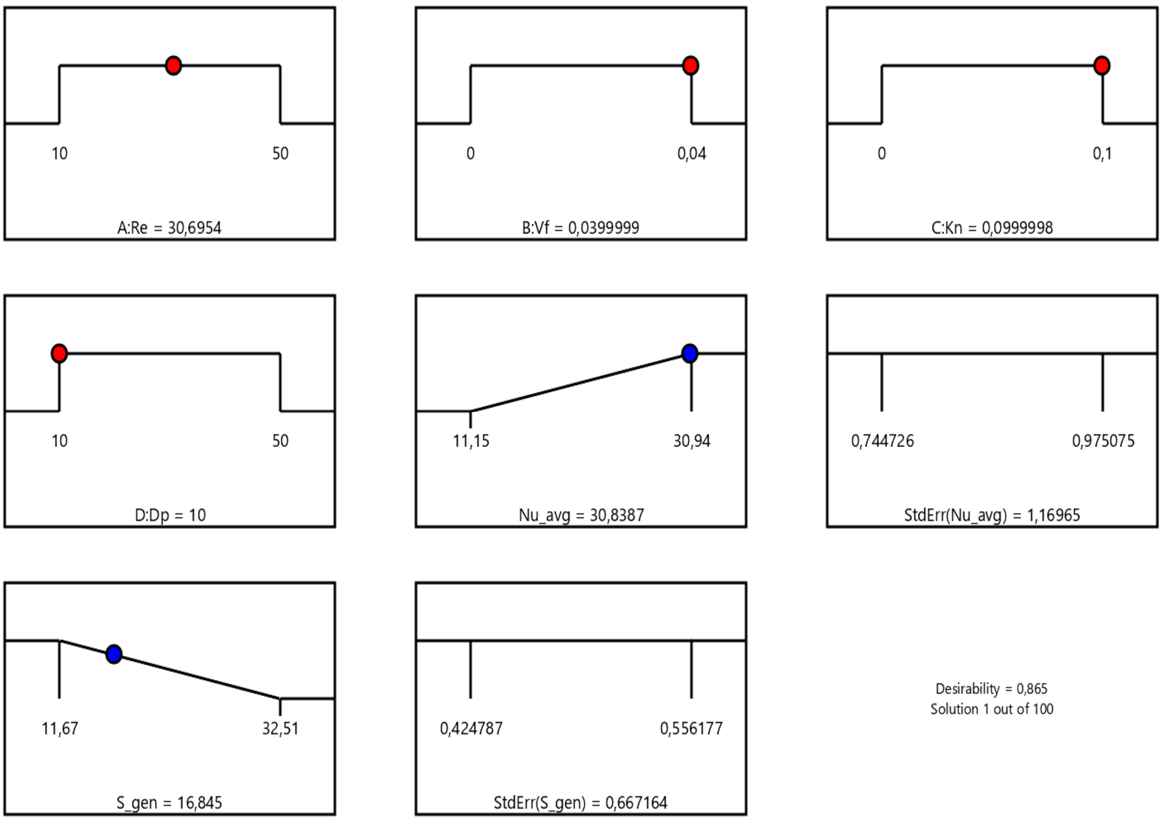

Micro-channel optimized model for optimal design factors

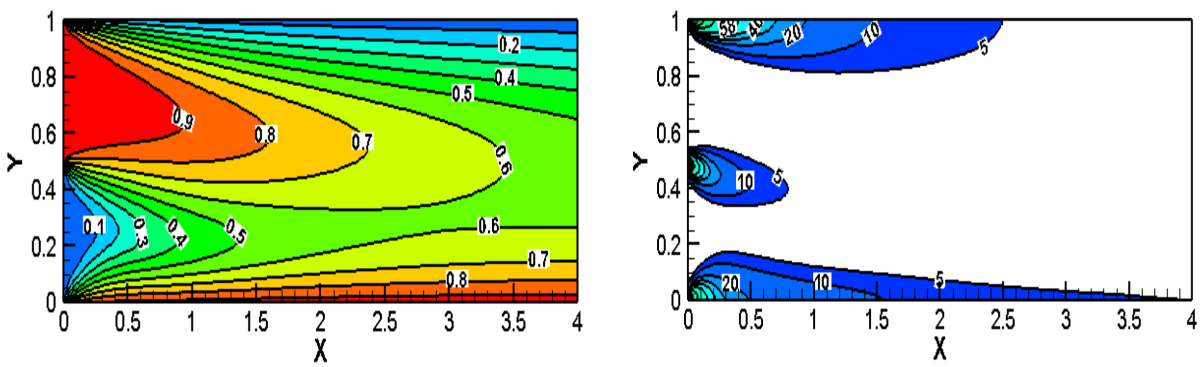

Figure 12. Isotherms (left) and entropy generation (right) for optimal design factors inside the micro-channel

7.3. AFTER-OPTIMIZATION ANALYSIS

A systematic optimization framework combining the Box-Behnken Design of Experiments (DoE) and Lattice Boltzmann Method (LBM) simulations delivers critical insights into thermal system performance. The process begins by determining optimal input parameters (*Re* = 30.7, *Kn*=0.1, *Vf*=0.04, and *Dp*=10), through DoE-driven optimization. These parameters are then applied in high-resolution LBM simulations, achieving a peak average Nusselt number (*Nu_max*) of 30.8811 and a reduced entropy generation rate (*S_gen*) of 16.7378, signifying an improvement in thermal efficiency over baseline systems.

A comparative evaluation of DoE predictions and LBM results demonstrates strong alignment, with minimal deviations: an absolute difference of 0.0424 (0.14%) in *Nu_avg* and 0.1 (0.63%) in *S_gen*. This close agreement validates both the DoE's predictive accuracy in modeling parameter interactions and the LBM's reliability in capturing complex thermal-fluid dynamics. The consistency between theoretical predictions and simulated outcomes confirms the framework's robustness in addressing nonlinear optimization challenges.

By bridging experimental design with computational precision, this methodology establishes a validated approach for optimizing thermal systems, paving the way for scalable engineering solutions in energy-intensive applications.

The surface distribution depicted in Figure 12 corresponds to the optimized configuration which gives *Nu_avg*=30.8811 and *S_gen*=16.7378.

8. CONCLUSION

This study successfully employed Response Surface Methodology (RSM), based on data from the numerical simulation realized by LBM, to optimize the performance of a co-flow micro-heat-exchanger, focusing on the simultaneous maximization of energy transfer rate and minimization of thermodynamic irreversibility. The developed numerical model accurately predicted the heat transfer and fluid flow characteristics within the microchannel, providing a robust foundation for RSM analysis. By resolving the limitations of prior works—such as neglecting rarefaction ([30]), oversimplifying nanofluids ([13]), and single-objective myopia ([10])—this study delivers an experimentally validated framework for Pareto-optimal micro-heat-exchanger design. The analysis of the independent impact of each design factor shows that when the Kn number rises, the movement of the particles in the core region becomes decelerated and increases near the side walls which affect directly on the slip velocity and temperature to jump. In addition, the increase of Re affects the thermodynamic structure of the co-flow through the micro-heat-exchanger. The optimization process identified conditions (Re=30.7, Kn=0.1, Vf=0.04, Dp=10) that prioritize heat transfer enhancement while curbing entropy generation, though these objectives remain partially conflicting. Designers must weigh Nu against S_gen based on application constraints. The results demonstrate the effectiveness of RSM as a powerful tool for efficient exploration of the design space and identification of optimal operating conditions for micro-heat-exchangers. The findings contribute valuable insights into the design and optimization of high-performance, energy-efficient micro-heat-exchangers for diverse applications, highlighting the crucial interplay between heat transfer enhancement and thermodynamic irreversibility reduction. Future work could explore the impact of other design variables, investigate different working fluids, or extend the analysis to consider more complex flow configurations. The optimized micro-heat-exchanger design directly addresses critical needs in electronics cooling, biomedical devices, and renewable energy systems. By validating LBM-RSM synergy for co-flow nanofluids, this work provides a scalable blueprint for industries prioritizing miniaturization, energy efficiency, and thermal stability.

CONFLICT OF INTEREST

The author(s) declared no potential conflicts of interest concerning the research, authorship, and publication of this article.

DATA AVAILABILITY

The datasets generated and/or analyzed during the current study are available within the paper.

REFERENCES

[1] A. Zeeshan, R. Ellahi, M.A. Rafique, S.M. Sait, N. Shehzad, Parametric optimization of entropy generation in hybrid nanofluid in contracting/ expanding channel by means of analysis of variance and response surface methodology, Inventions 9 (2024) 92.

[2] T. Mehmood, M. Ramzan, F. Howari, S. Kadry, Y.-M. Chu, Application of response surface methodology on the nanofluid flow over a rotating disk with autocatalytic chemical reaction and entropy generation optimization, Scientific Reports 11 (2021) 4021.

[3] S. Jawairia, J. Raza, Optimization of heat transfer rate in a moving porous fin under radiation and natural convection by response surface methodology: Sensitivity analysis, Chemical Engineering Journal Advances 11 (2022) 100304.

[4] A. Kazemian, M. Khatibi, T. Ma, Performance prediction and optimization of a photovoltaic thermal system integrated with phase change material using response surface method, Journal of Cleaner Production 290 (2021) 125748.

[5] T. Hayat, S.A. Khan, A. Alsaedi, Q.Z. Zai, Computational analysis of heat transfer in mixed convective flow of CNTs with entropy optimization by a curved stretching sheet, International Communications in Heat and Mass Transfer 118 (2020) 104881.

[6] M. Alhadri, J. Raza, U. Yashkun, L.A. Lund, C. Maatki, S.U. Khan, L. Kolsi, Response surface

methodology (RSM) and artificial neural network (ANN) simulations for thermal flow hybrid nano–fluid flow with Darcy-Forchheimer effects, Journal of the Indian Chemical Society 99 (2022) 100607.

[7] A.A. Ahmadi, M. Arabbeiki, H.M. Ali, M. Goo–darzi, M.R. Safaei, Configuration and optimization of a minichannel using water–alumina nanofluid by non-dominated sorting genetic algorithm and response surface method, Nanomaterials 10 (2020) 901.

[8] M.M. Ghorani, M.H.S. Haghighi, A. Riasi, Entropy generation minimization of a pump running in reverse mode based on surrogate models and NSGA-II, International Communications in Heat and Mass Transfer 118 (2020) 104898.

[9] S. Ontela, P.K. Pattnaik, S. Panda, S.R. Mishra, Optimizing heat transfer rate and sensitivity analysis of hybrid nanofluid flow over a radiating sheet: Applications in solar-powered charging sta–tions, Numerical Heat Transfer, Part B: Funda–mentals (2024) 1–21. https://doi.org/10.1080/10407790.2024.2341439.

[10] P.K. Pattnaik, S.R. Mishra, S. Panda, Response surface methodology on optimizing heat transfer rate for the free convection of micro-structured fluid through permeable shrinking surface, Eur. Phys. J. Plus 139 (2024) 221. https://doi.org/10.1140/epjp/s13360-024-05001-9.

[11] S.M. Javadpour, M. Dehghani, V. Mahmoudi, D. Toghraie, S. Salahshour, Optimization of nanofluid flow in a mini-channel with semi-porous fins using response surface methodology based on the Box–Behnken design, J Therm Anal Calorim (2024). https://doi.org/10.1007/s10973-024-13616-4.

[12] B. Almasri, T. Mohapatra, H. Joardar, S.S. Mishra, Experimental investigation and multi-objective optimization of a novel multi-fluid heat exchanger performances using response surface methodology and genetic algorithm, J Braz. Soc. Mech. Sci. Eng. 46 (2024) 400. https://doi.org/10.1007/s40430-024-04987-8.

[13] O.G. Fadodun, A.A. Amosun, N.L. Okoli, D.O. Olaloye, S.S. Durodola, J.A. Ogundeji, Sensitivity analysis of entropy production in Al2O3/H2O nanofluid through converging pipe, J Therm Anal Calorim 143 (2021) 431–444. https://doi.org/10.1007/s10973-019-09163-y.

[14] P.K. Tyagi, R. Kumar, Thermodynamic modeling and performance optimization of nanofluid-based photovoltaic/thermal system using central compo–site design scheme of response surface metho–dology, Renewable Energy 225 (2024) 120341.

[15] V. Akgül, B. Kurşuncu, H. Kaya, Response surface methodology-based multi-objective grey relation optimization for impinging jet cooling with Al_2O_3/water nanofluid on a curved surface, Neural Comput & Applic 35 (2023) 13999–14012. https://doi.org/10.1007/s00521-023-08357-8.

[16] J. Sun, R. Zhang, M. Wang, J. Zhang, S. Qiu, W. Tian, G.H. Su, Multi-objective optimization of helical coil steam generator in high temperature gas reactors with genetic algorithm and response sur–face method, Energy 259 (2022) 124976.

[17] M. Ferhi, D. Khilifi, R. Djebali, Heat Transfer and Irreversibility Response Due to Natural Convection in a Micro Partially Porous Cavity: Micro-Elec–tronic Cooling Application, in: 2023 14th Inter–national Renewable Energy Congress (IREC), IEEE, 2023: pp. 1–6.

[18] O.G. Fadodun, B.A. Olokuntoye, A.O. Salau, A.A. Amosun, Numerical investigation and sensitivity analysis of entropy generation of Al2O3/H2O na–nofluid in turbulent regime using response surface methodology, Archives of Thermodynamics (2020) 119–146.

[19] O.G. Fadodun, A.A. Amosun, N.L. Okoli, D.O. Olaloye, S.S. Durodola, J.A. Ogundeji, Sensitivity analysis of entropy production in Al2O3/H2O na–nofluid through converging pipe, J Therm Anal Calorim 143 (2021) 431–444. https://doi.org/10.1007/s10973-019-09163-y.

[20] S. NS, B.J. Gireesha, B. Mahanthesh, P. BC, A.J. Chamkha, Entropy generation analysis of magneto-nanoliquids embedded with aluminium and tita–nium alloy nanoparticles in microchannel with partial slips and convective conditions, Interna–tional Journal of Numerical Methods for Heat & Fluid Flow 29 (2019) 3638–3658.

[21] R. Djebali, A. Jaouabi, T. Naffouti, S. Abboudi, Accurate LBM appraising of pin-fins heat dissi–pation performance and entropy generation in enc–losures as application to power electronic cooling, International Journal of Numerical Methods for Heat & Fluid Flow 30 (2020) 742–768.

[22] M. Ferhi, R. Djebali, Heat transfer appraising and second law analysis of Cu-water nanoliquid filled microchannel: Slip flow regime, Romanian Journal of Physics 67 (2022) 605.

[23] R. Rabhi, B. Amami, H. Dhahri, A. Mhimid, Heat Transfer and Entropy Generation in Porous Mic–roduct with Slip Boundary Condition Using Lattice Boltzmann Method under Nonequilibrium Condi–tions, Journal of Porous Media 20 (2017).

[24] J. Baliti, M. Hssikou, Y. Elguennouni, A. Mous–saoui, M. Alaoui, Heat Transfer and Entropy Gene–ration for Natural Convection by Adiabatic Obs–tacles Inside a Cavity Heated on the Left Side., FME Transactions 48 (2020).

[25] F. Zair, M. Mouqallid, R. El Maani, The Effect of the Presence of Obstacles on the Emission Disper–sion Emitted by a Bent Chimney., FME Tran–sactions 48 (2020).

[26] P.K. Pattnaik, S.R. Mishra, S. Panda, Response surface methodology on optimizing heat transfer rate for the free convection of micro-structured fluid through permeable shrinking surface, Eur. Phys. J. Plus 139 (2024) 221. https://doi.org/10.1140/epjp/s13360-024-05001-9.

[27] R. Rabhi, A. Yahya, B. Amami, H. Dhahri, Inf–luence of magnetohydrodynamic viscous flow on

entropy generation within porous micro duct using the Lattice Boltzmann Method, RSC Advances 7 (2017) 30673–30686.

[28] M. Ferhi, R. Djebali, S. Abboudi, W. Al-kouz, Magnetohydrodynamic (MHD) convective nano–fluid flow, heat transfer and irreversibility analysis in a horizontal micro tall cavity with heat sources in the slip regime, Journal of Nanofluids 11 (2022) 510–527.

[29] A.S. Lobasov, A.V. Minakov, The investigation of the height effect of a slit microchannel with a textured wall on its hydrodynamic drag, in: Journal of Physics: Conference Series, IOP Publishing, 2021: p. 012050.

[30] A. Raisi, B. Ghasemi, S.M. Aminossadati, A Nu–merical Study on the Forced Convection of La–minar Nanofluid in a Microchannel with Both Slip and No-Slip Conditions, Numerical Heat Transfer, Part A: Applications 59 (2011) 114–129. https://doi.org/10.1080/10407782.2011.540964.

[31] S. Marzougui, F. Mebarek-Oudina, M. Magherbi, A. Mchirgui, Entropy generation and heat transport of Cu–water nanoliquid in porous lid-driven cavity through magnetic field, HFF 32 (2022) 2047–2069. https://doi.org/10.1108/HFF-04-2021-0288.

[32] W. Al-Kouz, A. Al-Muhtady, W. Owhaib, S. Al-Dahidi, M. Hader, R. Abu-Alghanam, Entropy ge–neration optimization for rarified nanofluid flows in a square cavity with two fins at the hot wall, Entropy 21 (2019) 103.

[33] M.A. Abbassi, J. Orfi, Effects of Magnetohydro–dynamics on Natural Convection and Entropy Ge–neration with Nanofluids, Journal of Thermo–physics and Heat Transfer 32 (2018) 1059–1071. https://doi.org/10.2514/1.T5343.

[34] Y. Oulahou, Y. Elguennouni, M. Hssikou, J. Baliti, M. Alaoui, Numerical Investigation of Natural Convection Heat Transfer Using TiO 2/Al 2 O 3-Water Nanofluids., FME Transactions 52 (2024).

[35] Q. Zou, X. He, On pressure and velocity boundary conditions for the lattice Boltzmann BGK model, Physics of Fluids 9 (1997) 1591–1598.

[36] A. Mohamad, Lattice Boltzmann method funda–mentals and engineering applications with com–puter codes, Dept. of mechanical and manufac–turing engineering, Schulich School of Engineering, the University of Calgary, Alberta, Canada, Schulich School of Engineering, the University of Calgary, Alberta, Canada (2011).

[37] Z.-W. Tian, C. Zou, Z.-H. Liu, Z.-L. Guo, H.-J. Liu, C.-G. Zheng, Lattice Boltwmann method in simulation of thermal micro-flow with te;perature jump, Int. J. Mod. Phys. C 17 (2006) 603–614. https://doi.org/10.1142/S0129183106009187.

[38] S.B. Çelik, Analysis of single phase fluid flow and heat transfer in slip flow regime by parallel imp–lementation of lattice Boltzmann method on GPUS, Master's Thesis, Middle East Technical University (Turkey), 2012.

[39] T. Naffouti, R. Djebali, Natural convection flow and heat transfer in square enclosure asymetrically heated from below: A lattice Boltzmann comp–rehensive study, Computer Modeling in Engi–neering & Sciences(CMES) 88 (2012) 211–227.

[40] G.H. Tang, W.Q. Tao, Y.L. He, Simulation of fluid flow and heat transfer in a plane channel using the Lattice Boltwmann method, Int. J. Mod. Phys. B 17 (2003) 183–187. https://doi.org/10.1142/S0217979203017485.

[41] R. Mohebbi, M.M. Rashidi, M. Izadi, N.A.C. Sidik, H.W. Xian, Forced convection of nanofluids in an extended surfaces channel using lattice Boltzmann method, International Journal of Heat and Mass Transfer 117 (2018) 1291–1303.

[42] F. Durst, Fluid Mechanics: An Introduction to the Theory of Fluid Flows, Springer Berlin Heidelberg, Berlin, Heidelberg, 2022. https://doi.org/10.1007/978-3-662-63915-3.

NOMENCLATURE

LBM	Lattice Boltzmann Method
SRT-BGK	Single Relaxation Time-Bhatnagar-Gross-Krook
DOE	Design of experiments
MEM	Micro-Electro-Mechanical Systems
MHE	micro-heat-exchangers
HVAC	Heating Ventilation and Air-Conditioning
GPU	Graphics Processing Unit
RSM	Response Surface Methodology
Be	Bejan number
c	Lattice speed
c_s	Lattice speed of sound
c_k	Discrete particle speed
f, f^{eq}	Density distribution functions and its equilibrium part
F_k	External force
g, g^{eq}	Temperature distribution function and its equilibrium part
$\vec{g}$	Gravitational field (m. s^{-2})
k	Thermal conductivity ($W^{m-1}K^{-1}$)
H	Height
L	Length
Kn	Knudsen number
Re	Reynolds number
Nu	Local Nusselt number
Nu_av	Average Nusselt number
p	Pressure, (Pa)
Pr	Prandtl number = υ / α
T	Temperature, (K)
t	Time, (s)
ω_k	Weight factor
Vf	Nanoparticles volume fraction
u, v	Dimensional velocities, (m. s^{-1})
Cp	Heat capacitance
C_{jump}	Temperature jump coefficient

T_{jump}	Temperature jump
U_{slip}	Slip velocity
d_p	Nanoparticles diameter
$S_{\_gen}$	Total entropy production (W/m²K)
S_θ	Entropy due to heat transfer
S_f	Entropy due to fluid friction
υ	Kinematic viscosity, (m^2s^{-1})
τ	Dimensionless time
σ	Tangential momentum accommodation coefficient
ζ	Thermal accommodation coefficient
γ	Specific heat transfer ratio

Greek symbols

α	Thermal diffusivity, (m^2s^{-1})
β	Coefficient of thermal expansion, (K^{-1})
Δx	Lattice spacing
Δt	Time increment, (s)
μ	Dynamic viscosity, (kg $m^{-1}s^{-1}$)
ρ	Density, (kg m^{-3})
τ_α	Relaxation time for temperature, (m^2s^1)
τ_υ	Relaxation time for flow, (m^2 s^{-1})

Superscripts

c	Cold surface
h	Hot surface
s	Solid
p	Particle
nf	Nanofluid
in	Inlet

ОПТИМИЗАЦИЈА ПЕРФОРМАНСИ МИКРО-ИЗМЕЊИВАЧА ТОПЛОТЕ СА СУПРОТНИМ ПРОТОКОМ КОРИШЋЕЊЕМ МЕТОДОЛОГИЈЕ ПОВРШИНЕ ОДЗИВА: БРЗИНА ПРЕНОСА ЕНЕРГИЈЕ И ТЕРМОДИНАМИЧКА НЕПОВРАТНОСТ

М. Ферхи, Б. Млики, Р. Мири, Р. Ђебали

Овај рад истражује оптимизацију брзина преноса енергије и минимизирање термодинамичке неповратности у микро-каналном измењивачу топлоте са супротним протоком коришћењем методологије површине одзива (RSM) заједно са Box-Behnken дизајном експеримената. Развијен је сурогатни модел за корелацију критичних улазних параметара - укључујући Рејнолдсов број (Re), Кнудсенов број (Kn), запремински удео (Vf) и пречник честица (Dp) - са одговорима система: просечним Нуселтовим бројем (Nu_avg) и генерисањем ентропије (S_gen). Студија експлицитно бави ефектима услова протока на улазу на термичке перформансе анализирајући механизме присилне конвекције вођене смицањем. Као што је истакнуто у граничним условима, градијенти брзине на улазу стварају окружење у којем доминира мешање, где Рејнолдсов број (Re) управља динамиком флуида и преносом топлоте. Ово мешање побољшано смицањем значајно побољшава топлотни транспорт, док температурни градијенти на улазу доприносе локализованој размени топлоте између доње и горње површине канала. Утицаји улазних параметара се процењују кроз профиле брзине, брзину клизања, скок температуре, брзине преноса топлоте и стварање ентропије. Интеракција између ових фактора открива да већи Re (повезан са повећаним брзинама на улазу) интензивира конвективни пренос топлоте, али такође повећава вискозну дисипацију, представљајући компромис између Nu_avg и S_gen. RSM оптимизација идентификује Парето-оптималне услове који максимизирају пренос топлоте, а минимизирају неповратност. Анализа варијансе (ANOVA) потврђује значај сваког параметра, дајући регресионе једначине за Nu_avg и S_gen. Резултати показују ефикасност RSM-а у балансирању конкурентских циљева, нудећи практичне увиде за пројектовање високоефикасних микроканалних измењивача топлоте у апликацијама које захтевају прецизно управљање топлотом уз минималне губитке енергије. Овај рад наглашава критичну улогу услова улазног протока у диктирању перформанси микроканала, премошћујући јаз између идеализованих модела и практичних оперативних ограничења.